PROCEEDINGS OF SPIE

SPIEDigitalLibrary.org/conference-proceedings-of-spie

Testing and characterization of the TESS CCDs

C. Thayer, J. Villasenor, S. Kissel, B. LaMarr, E. Morgan, et al.

C. Thayer, J. Villasenor, S. Kissel, B. LaMarr, E. Morgan, G. Prigozhin, I. Prigozhin, G. Ricker, T. Sauerwein, V. Suntharalingam, R. Vanderspek, D. Woods, "Testing and characterization of the TESS CCDs," Proc. SPIE 9904, Space Telescopes and Instrumentation 2016: Optical, Infrared, and Millimeter Wave, 99042X (29 July 2016); doi: 10.1117/12.2232886

SPIE.

Event: SPIE Astronomical Telescopes + Instrumentation, 2016, Edinburgh, United Kingdom

Testing and characterization of the TESS CCDs

C. Thayer[1], J. Villasenor[1], S. Kissel[1], B. LaMarr[1], E. Morgan[1], G. Prigozhin[1], I. Prigozhin[2], G. Ricker[1], T. Sauerwein[1], V. Suntharalingam[2], R. Vanderspek[1], D. Woods[2]

[1]MIT Kavli Institute for Astrophysics and Space Research
[2]MIT Lincoln Laboratory

ABSTRACT

The Transiting Exoplanet Survey Satellite (TESS) is an Explorer-class mission dedicated to finding planets around bright, nearby stars so that more detailed follow-up studies can be done. TESS is due to launch in 2017 and careful characterization of the detectors will need to be completed on ground before then to ensure that the cameras will be within their photometric requirement of 60ppm/hr. TESS will fly MIT-Lincoln Laboratories CCID-80s as the main scientific detector for its four cameras. They are 100μm deep depletion devices which have low dark current noise levels and can operate at low light levels at room temperature. They also each have a frame store region, which reduces smearing during readout and allows for near continuous integration. This paper describes the hardware and methodology that were developed for testing and characterizing individual CCID-80s. A dark system with no stimuli was used to measure the dark current. Fe^{55} and Cd^{109} X-ray sources were used to establish gain at low signal levels and its temperature dependence. An LED system that generates a programmable series of pulses was used in conjunction with an integrating sphere to measure pixel response non-uniformity (PRNU) and gain at higher signal levels. The same LED system was used with a pinhole system to evaluate the linearity and charge conservation capability of the CCID-80s.

Keywords: CCD, dark current, gain, pixel response non-uniformity, linearity, TESS, exoplanets

1. INTRODUCTION

The Transiting Exoplanet Survey Satellite (TESS) is a NASA explorer-class mission whose primary goal is to detect Earth-like planetary systems around nearby stars that will be the subject of follow up studies from space and ground-based telescopes (Ricker *et al.,* 2014). It is a MIT Kavli Institute (MKI) project in collaboration with MIT Lincoln Laboratory, NASA's Goddard Spaceflight Center, Orbital ATK, NASA's Ames Research Center, the Harvard-Smithsonian Center for Astrophysics, the Aerospace Corporation, and the Space Telescope Science Institute.

There will be a single scientific instrument on TESS, consisting of 4 cameras, each of which will contain an array of four MIT/LL CCID-80 detectors in the focal plane of a custom 145mm, f/1.46 optic. The CCID-80s are deep-depletion, back-illuminated, frame-store devices designed and fabricated at MIT Lincoln Laboratory (Suntharalingam *et al.*, 2016). The image array is 2048 rows by 2048 columns with a pixel size of 15μm and a depletion depth of 100μm. The high depletion depth of the CCDs enables the wide nandpass of the TESS camera (600-1050nm). The frame-store is the same size as the image array, and allows the image to be transferred out of the image array in 20ms before is it read out more slowly (1.8s) through the electronics. A thin (250 nm) layer of aluminum covers the frame-store region, blocking any optical light from the pixels below, while an antireflection coating is deposited on the imaging array region to improve CCD quantum efficiency. The CCD is read out through four output nodes at a rate of 625 pixels/s.

This paper discusses the methods and techniques we have used to determine the read noise, dark current, pixel response non-uniformity (PRNU), gain, linearity, full well, and charge conservation of the CCID-80s.

Space Telescopes and Instrumentation 2016: Optical, Infrared, and Millimeter Wave, edited by Howard A. MacEwen, Giovanni G. Fazio, Makenzie Lystrup, Proc. of SPIE Vol. 9904, 99042X · © 2016 SPIE · CCC code: 0277-786X/16/$18 · doi: 10.1117/12.2232886

2. HARDWARE

Because the performance of these CCDs is dependent on temperature they were tested over an extended temperature range centered on the operating temperature, nominally -60°C. A vacuum testing chamber was designed for testing individual CCDs (see Figure 1). The CCD is mounted to a liquid-nitrogen-cooled cold plate within the chamber. The chamber has an optical flat window to allow for testing with optical light and a 25μm thick beryllium window to enable testing with Iron-55 (Fe^{55}) and Cadmium-109 (Cd^{109}) X-ray sources. The temperature of the CCD was measured by a platinum resistance temperature detector (RTD) that is attached to the CCD mount. The electronics are within the chamber and are thermally isolated from the CCD, keeping their operational temperature above -20°C.

Figure 1. The vacuum chamber designed to testing of CCID-80s at MKI. a) Optical window b) Beryllium window

2.1 CCD Readout

For the data presented in this paper, pre-flight electronics were used with a flight-grade engineering CCD and an exposure time of 2 seconds. The frame readout sequence used here is similar to the one used for flight (see Figure 2). At the top of each frame there are 10 buffer rows that are at the edge of the CCD and get integrated along with the data rows. Following the buffer rows, there are 10 smear rows that consist of pixels that do not integrate in the CCD but are transferred through both in the image array and the frame-store during the frame transfer. After the smear rows, there are 10 virtual rows, which consist of pixels that are only transferred through the frame-store and are not exposed to any illumination. Once the pixels reach the serial register, each output is read out individually. Each row that passes through a readout node begins with 11 pre-scan pixels, that are read through the electronics but not through the CCD, followed by 512 data pixels, and then by 11 overclock pixels, that are read through the serial register of the CCD and the electronics but not through the collection area of the CCD.

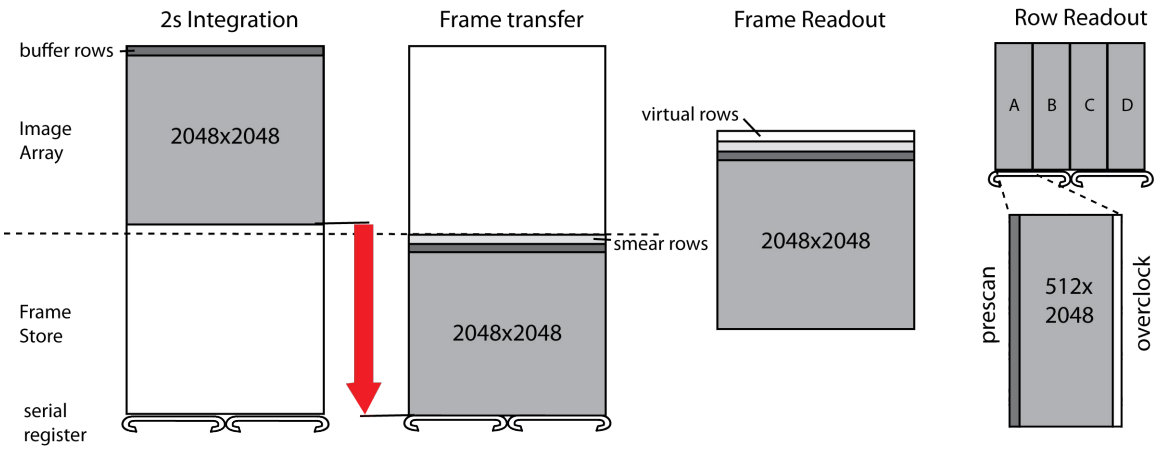

Figure 2. The readout sequence of a CCD. The image array and buffer rows integrate for 2s before they are transferred to the frame store creating the smear rows by overclocking 10 rows. They are then transferred through the frame store, creating virtual rows by overclocking by 10 rows. Each row is transferred into the serial register and then read out. As each row is read out it is preceded by 11 prescan pixels and followed by 11 overclock pixels. Not to scale.

2.2 Optical Illumination

There are two types of optical illumination we used: flood illumination that shines light on the whole CCD and point source illumination which shines a tight, focused spot on a single output of the CCD at a time. To produce the flood illumination, we used an LED illuminated Thorlabs 6" integrating sphere with 1" diameter ports. The intensity of the light is driven by pulsing (Agilent 33500 B Waveform Generator) the LED. The pulser is triggered by the start-of-frame signal coming out of the data line to begin a train of pulses during the integration period. The pulser is computer-controlled to produce specified numbers of pulses in an automated fashion (see Figure 3). The repeatability and reliability of the system was validated by measuring the output of the pulser with an oscilloscope.

For point source illumination, we replace the integrating sphere with a lens doublet system that produces a focused spot with a width of 2 to 3 pixels. At one end of the system there is a 5 μm pinhole coupled and centered to an LED illuminated optical fiber. The lens system consists of two doublets, both with diameter of 2", one with f=200mm and one with f=300mm. There are x, y, and z translation stages for focus and to move the location of the spot across the CCD so that it can land on all four outputs.

We used 3 different thermally stable, fiber-coupled LEDs from Thorlabs for both the flood illumination and the point source illumination. The wavelengths of the LEDs were 660nm and 850nm, both with a 50nm bandpass, and 1050nm with a 150nm bandpass. The optical range of TESS is 600nm to 1050nm.

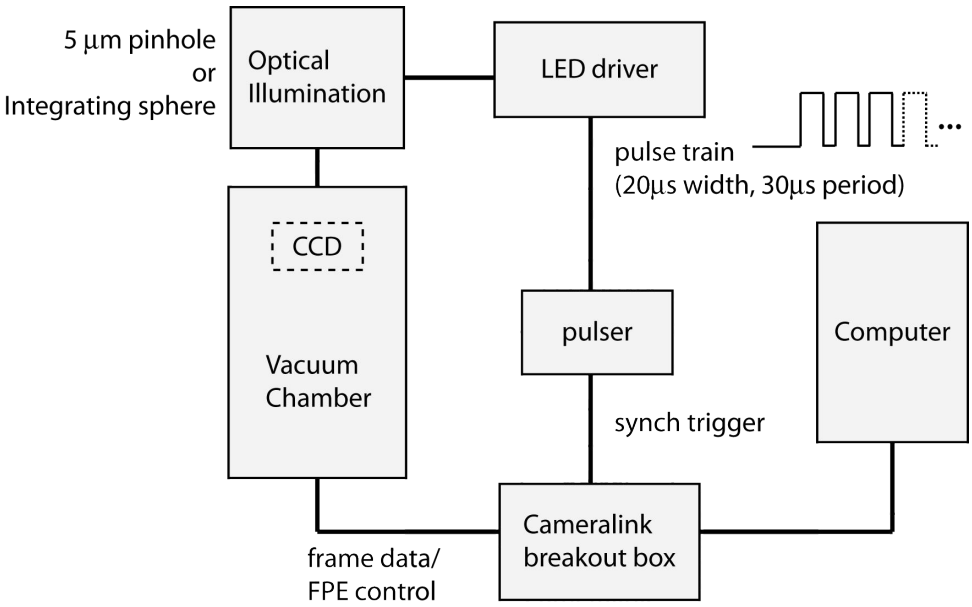

Figure 3. The block diagram of the optical testing system. There are two options for the Optical Illumination block, either a 5µm pinhole for the point source illumination or an integrating sphere for the flood illumination.

2.2 X-ray Illumination

Although TESS is not an X-ray mission, we utilized the fact that the precise energy level of the illumination is known for X-ray data to calibrate the gain of the CCD. We alternately shone Fe^{55} and Cd^{109} on the CCD through a beryllium window. The CCD is far enough away from the window that there is an even spread of X-rays across the CCD. The MKI CCD Lab has used Fe^{55} extensively for low-level gain calibration for X-ray missions such as Chandra and AstroE (Grant *et al.*, 2014). Cd^{109} was added because it has a higher photon energy to increase the measurement accuracy.

3. CHARACTERISTIC ANALYSIS

4.1 Read Noise

Read noise is the noise on the output node, so each of the 4 outputs of a CCD has different read noise measurements. The overclock pixels at the end of each row were used to calculate the read noise for each output because they were read out through the output node and contain the read noise but they did not have any signal from the imaging pixels. The standard deviation of the overclock pixels for a given output was used as the read noise value for that ouput. The average read noise value for a CCID-80 attached to the pre-flight electronics was measured to be 14 electrons (e-). Preliminary tests of flight electronics show this value to be 7-9 e-.

4.2 Dark Current

The CCID-80s have sufficiently low enough dark current that they can image at room temperature without saturating. Dark room temperature images consistently show a "brickwall" pattern (see Figure 4), which was a result of the ion implant/laser annealing process done to passivate each surface of the CCDs and reduce the dark current (Westhoff *et al*., 2009). The pattern follows the laser treatment as it was stepped across the surface of the CCD. This feature disappears at -20C but was useful as an aliveness check before cooling the CCD.

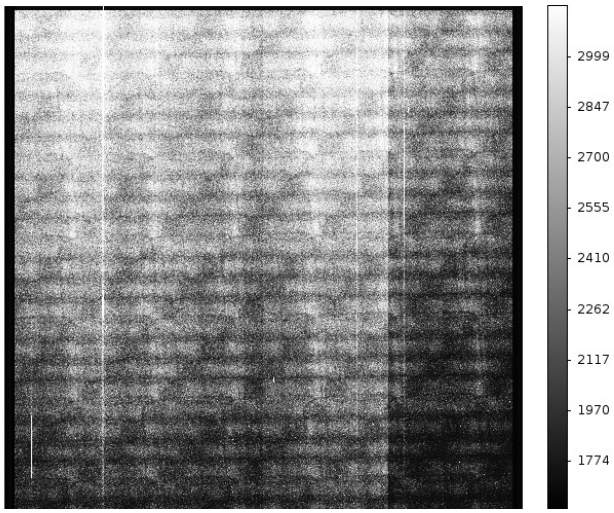

Figure 4. The "brickwall" pattern at room temperature. The average difference in signal level between the light and the dark areas is 615 ADU (Analogue to Digital readout Units). The signal levels shown in the scale bar are in ADU.

We utilized the virtual rows at the top of dark frames to measure the dark current. After subtracting off the read noise and shot noise from the frames, we stacked 100 2-second frames together. We averaged the columns in the virtual rows and the columns in 10 rows of the integrated image array and subtracted the two (see Figure 5). By subtracting them we removed the systematic start of line ringing that the electronics produced (The start of line ringing was due to the power supply fluctuations in the video chain of the electronics boards and are stationary and hence can reliably be subtracted off. The amplitude of this feature will be substantially reduced on flight boards.) and leave behind the dark current that accumulated during integration. Stacking effectively measured the dark current collected over 3.3 hours. We repeated this on dark frames taken at varying temperatures in order to get the temperature dependence of the dark current. The measured levels begin to flatten at -60C (see Figure 6) limited by a light leak level in our setup. Using an exponential fit of the data we found the doubling temperature of the dark current in a CCID-80 to be 5.5 ± 0.1C.

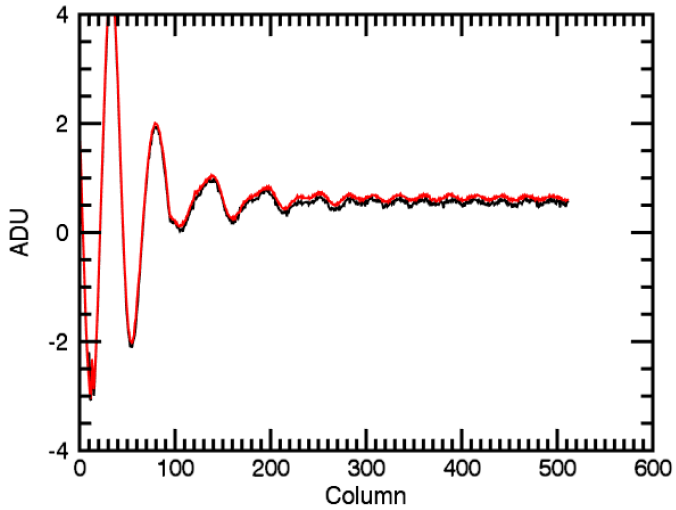

Figure 5. The signal across a row in a dark image (black – virtual rows, red – integrated image array). The difference between the signal levels is the dark current. The amplitude of the start of line ringing varies from channel to channel and currently the lowest is a factor of 2 less than shown here. In flight electronics it will be ±0.5 ADU.

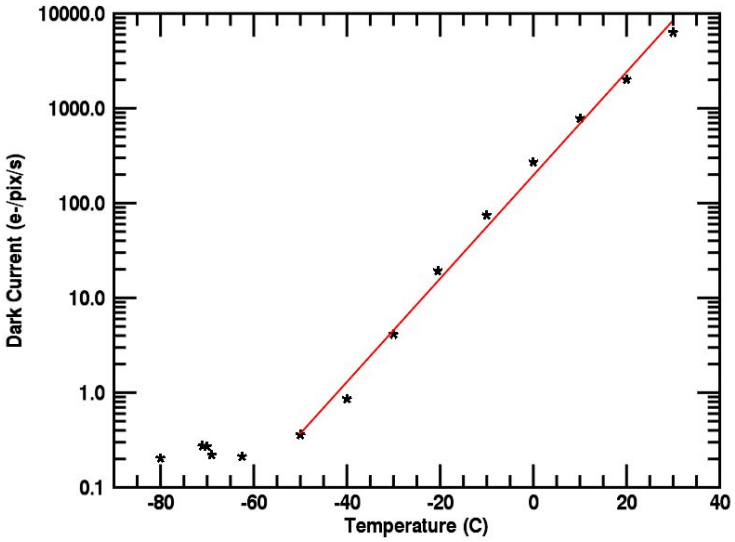

Figure 6. Dark current as a function of temperature. A light leak in our setup limits our measurements to 0.25 e-/pix/s. The measured dark current at room temperature matches the average signal level in the brickwall images in Figure 4.

4.3 Pixel Response Non-Uniformity (PRNU)

A measure of the pixel response non-uniformity (PRNU) is important for the proper calibration of the data collected on orbit, so a map of the non-uniformity across each output of a CCD was created. The signal (S) in a frame after the background is subtracted is the product of the pixel-to-pixel variation (PRNU) and the illumination (I) (see Equation 1) (Janesick, 2001).

$$S(x,y) - Dark(x,y) = PRNU(x,y) * I(x,y) \quad (1)$$

To extract the PRNU, we stacked 2,500 frames of the background-subtracted flood data, each frame with ~100,000 e^-. We then created a fit for the illumination using a low-pass filter, averaging over 80x80 pixels, centered on each pixel. We divided the stacked image by the illumination fit and the residual is the PRNU (see Figure 7) with a sigma of 0.7% (see Figure 8). We fit the illumination level and produced the PRNU for each of the 4 outputs individually and then stitched them together to create one PRNU for a CCD.

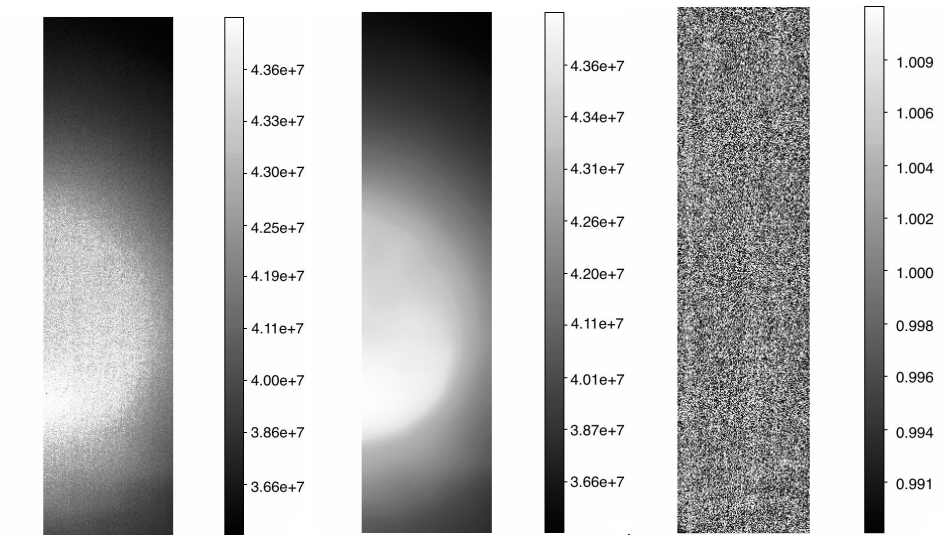

Figure 7. Left: the background-subtracted stacked frame for a single output of the CCD. Center: the low-pass filter illumination fit. Right: the residual PRNU. All values are in ADU. Data taken at 660nm.

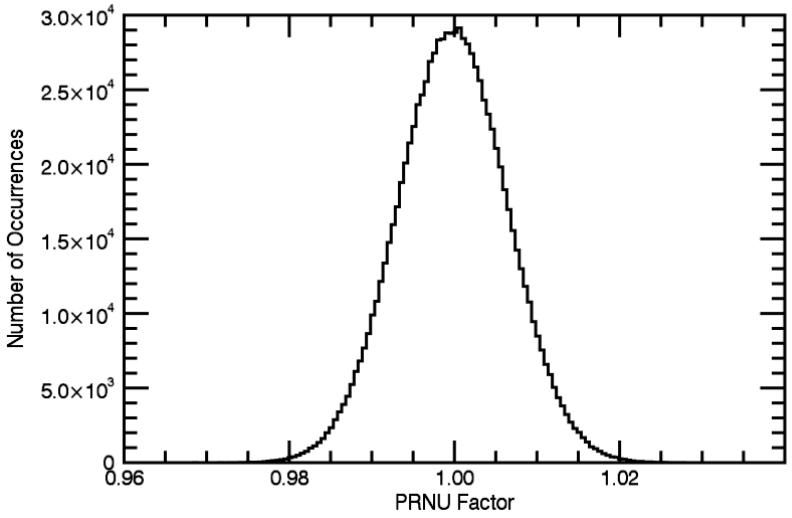

Figure 8. Histogram of the PRNU for a single output. The 1-sigma width of this distribution of 0.7%

In order to ensure that we had the best filter size possible we created a randomly generated PRNU and multiplied it by a generated polynomial illumination fit to create a dummy stacked frame with known components. The PRNU extraction was run on the dummy stacked frame with a range of filter size from 10 pixels to 100 pixels. A filter size of 80 pixels produced a PRNU closest to the starting PRNU and was set as the default filter size to make PRNUs.

The PRNU shows two features of the CCID-80s that are hidden by other signals in standard frames (see Figure 9). The laser annealing process that created the brickwall pattern in the dark current also generated a similar pattern in the quantum efficiency of the CCD. The curved arcs across a detector are a phenomenon known as tree rings. They were caused during the manufacturing of the silicon wafer that the CCD was made from. Doping inhomogeneities present during the refinement process of the silicon boule, from which

the CCD wafers are cut, cause lateral fields that deflect the charge generated by incoming photons (Green *et al*., 2013).

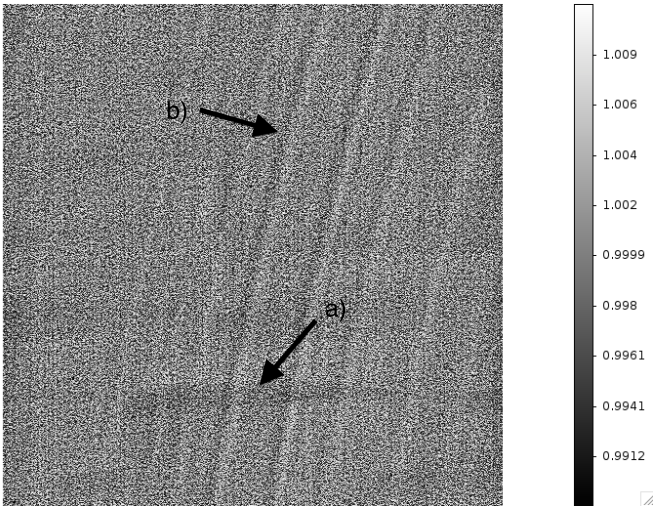

Figure 9. a) Laser annealing pattern. b) Tree rings.

4.4 Gain

To properly measure how bright the stars are that TESS will be looking at we must accurately know the conversion between ADU, the Analogue to Digital readout Units, and electrons. At low signal levels (~1% of the CCD range) we use X-rays to measure the gain while we use a photon transfer curve done with flood illumination to measure the gain at higher signal levels (~50% of the CCD range).

4.4.1 X-ray

In order to obtain the gain using X-rays, we measured the signal levels of the K_α and K_β peaks from Fe^{55} and Cd^{109} (see Figure 10). To ensure that we were not losing any of the charge, we only used grade 0 events in our measurement, ones where all of the charge fell on one pixel. Using the known energies of the X-ray peaks (Fe^{55}: $K\alpha$ =5.9 keV, $K\beta$ = 6.5 keV, Cd^{109}: $K\alpha$ =22.1 keV, $K\beta$ = 25.0 keV) and the conversion of 3.65 eV/e- in silicon, we fit a line to the peaks whose slope was the gain conversion factor. This measurement must be done for each of the four outputs of a CCD. For the CCD that was used for the results in this paper with the engineering electronics at nominal operating temperature (-70C), the average gain was 6.95 ± 0.01 e-/ADU.

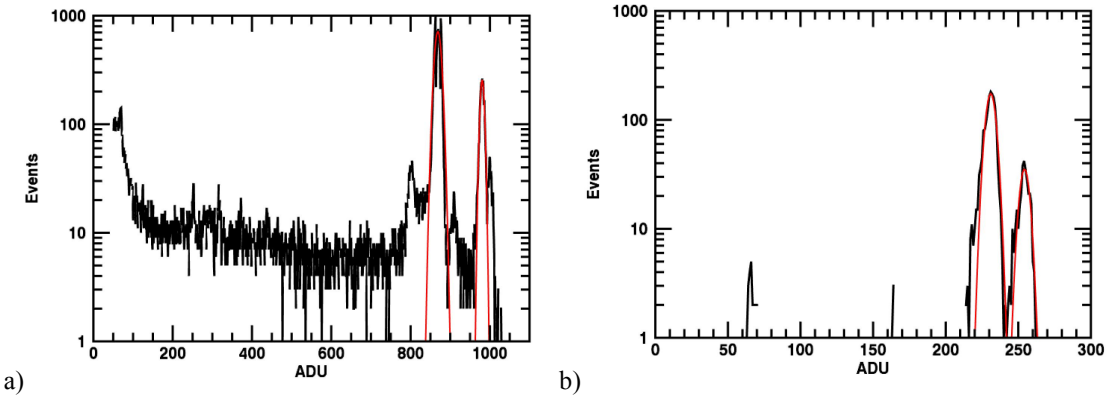

Figure 10. a) K_α and K_β peaks for Cd^{109}. b) K_α and K_β peaks for Fe^{55}.

4.4.2 Photon Transfer Curves

To measure gain optically we created a photon transfer curve (PTC), starting at very low signal levels and going up past full well. Gain can found using Equation 2 (Janesick, 2007) where S is the mean signal in ADU and σ_S is the noise of the signal in ADU.

$$Gain = \frac{S}{\sigma_S^2} \tag{2}$$

By removing the read noise and fixed pattern noise from the data before plotting the PTC, we could get the gain from the inverse of the slope of the PTC. However the increased charge sharing between pixels at high signal levels leads to error in signal measurement, which shifts the gain artificially (Guyonnet *et al.,* 2015). We corrected for this using the auto-correlation process described by Downing (2006), but we only found this valid for signal levels up to 10,000 ADU. The average gain we obtained through this process for each of the CCD outputs was 6.9 ± 0.1 e-/ADU (see Figure 11).

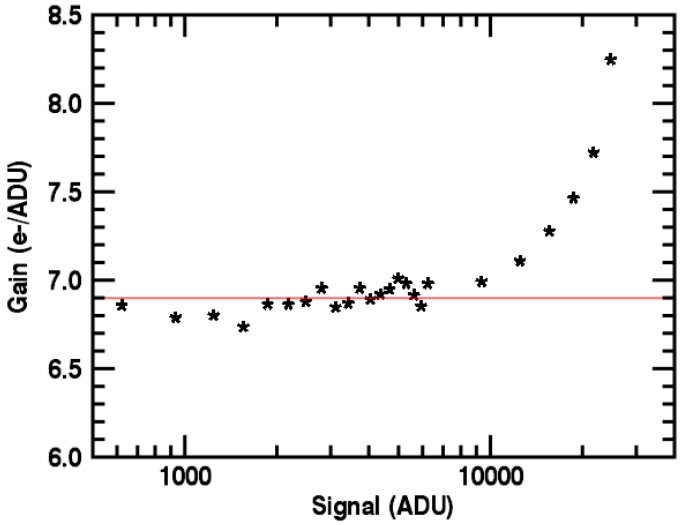

Figure 11. Gain as a function of signal level. Above 10,000 ADU the validity of this method of measuring gain begins to deteriorate because of increased charge sharing between pixels.

4.4.3 Temperature Dependence

Gain is a CCD characteristic that varies slightly with temperature. We used the X-ray data taken between -80C and -40C to determine the degree to which the gain changes with temperature (see Figure 12). We measured the dependence to be 0.0016 ± 0.0002 e-/ADU/K or 214 ± 27 ppm/K. A similar measurement done with optical data yields a dependence of 279 ± 79 ppm/K.

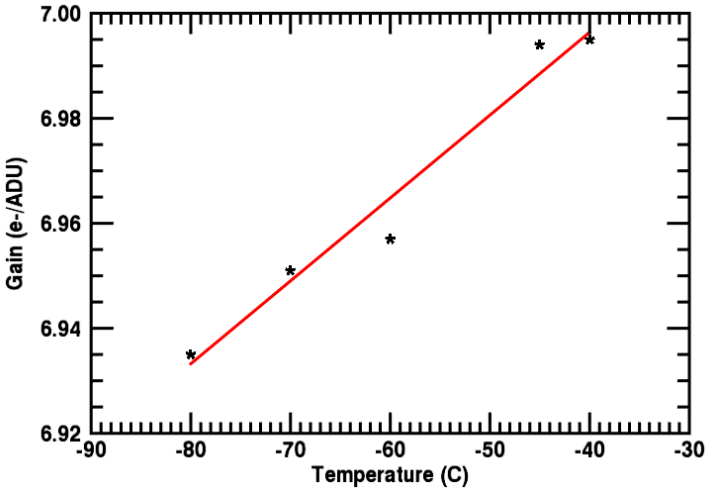

Figure 12. Gain as a function of temperature using X-rays to measure gain.

4.5 Linearity

To measure the linearity of the CCD, we took background-subtracted flood data and plotted the signal level against the input intensity (see Figure 13). We then did a linear fit of the data points between 50e- and 100,000 e-. We used the percent deviation of all of the data from the linear fit as our metric of linearity for the CCD. The CCID-80s are linear to within 0.3% through 150,000 e- and within 1% through 175,000 e- (see Figure 14).

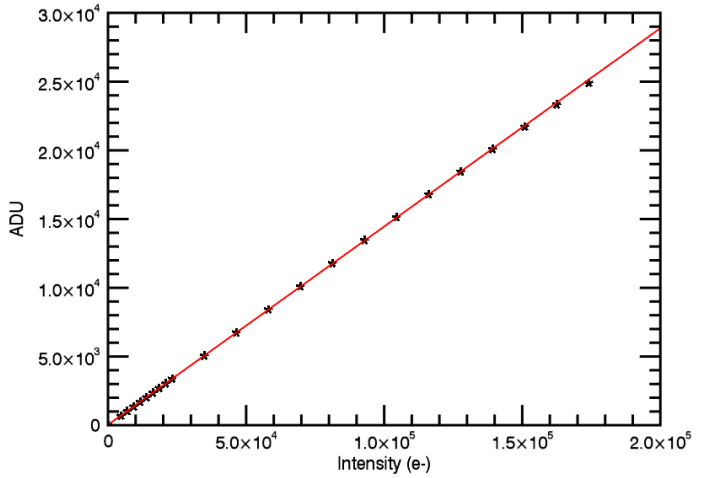

Figure 13. Measured signal level vs. input intensity. The red line is a linear fit of the data.

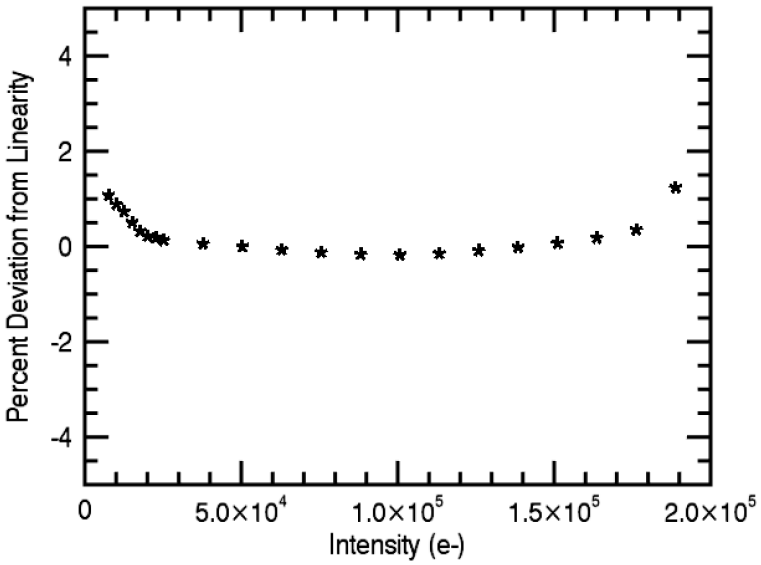

Figure 14. The percent non-linearity as a function of intensity.

4.6 Full Well

The full well capacity was measured using the optical point source: the intensity was increased until full well was reached and the charge began to spread into adjacent pixels. The full well capacity of the CCID-80s is dependent on the substrate bias voltage: this voltage ensures that the CCDs' depletion depth reaches the back surface. Although the devices are fully depleted when the substrate bias voltage is set to -25V or lower, the full well level varies past that point. The full well was measured at various levels of substrate bias voltage between -10V and -50V. As we decreased the substrate bias voltage the full well capacity increased until it reached a plateau of 250,000 e- (see Figure 15).

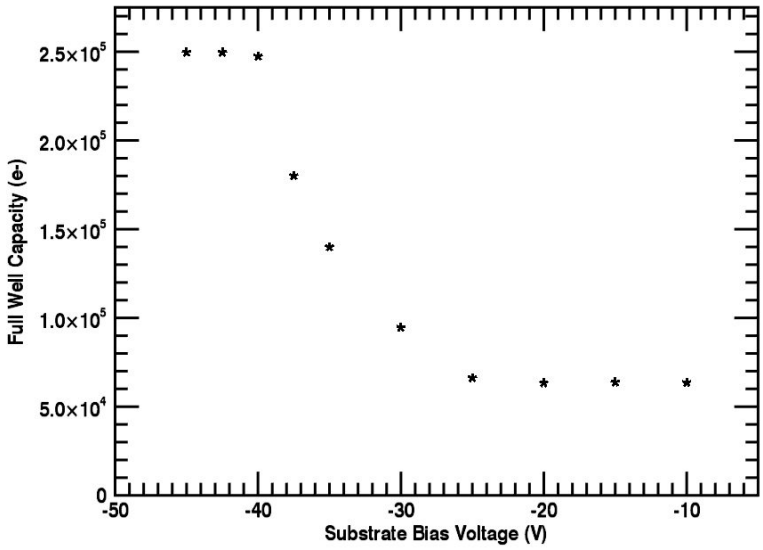

Figure 15. Full well as a function of substrate bias voltage.

4.7 Charge Conservation

In the TESS mission, there is a desire that photometry on stars as bright as I=2 can be performed to high accuracy. A source that bright will generate ~30 Me-, half of which will fall on the central pixel. The signal

in that central pixel will exceed the full well capacity by >100x and will therefore bloom over multiple pixels. The CCID-80 has no anti-blooming feature, so bloomed charge will be conserved up to a certain brightness: the intensity of a bloomed image can be accurately measured, provided a sufficient number of pixels is summed. We demonstrated charge conservation by increasing the intensity of a focused spot at 660nm, and measuring the total charge in a background-subtracted box sum (see Figure 16). A simple aperture consisting of 299x299 pixels was used to account for the spillage along columns. In this example, the average deviation of the data from a linear fit was 0.07% using intensities up to a total of 72.6Me- (I=1.1). However, because the level of charge conservation is a function of the substrate bias voltage, the brightness limit for charge conservation for the flight CCDs will be determined during instrument calibration.

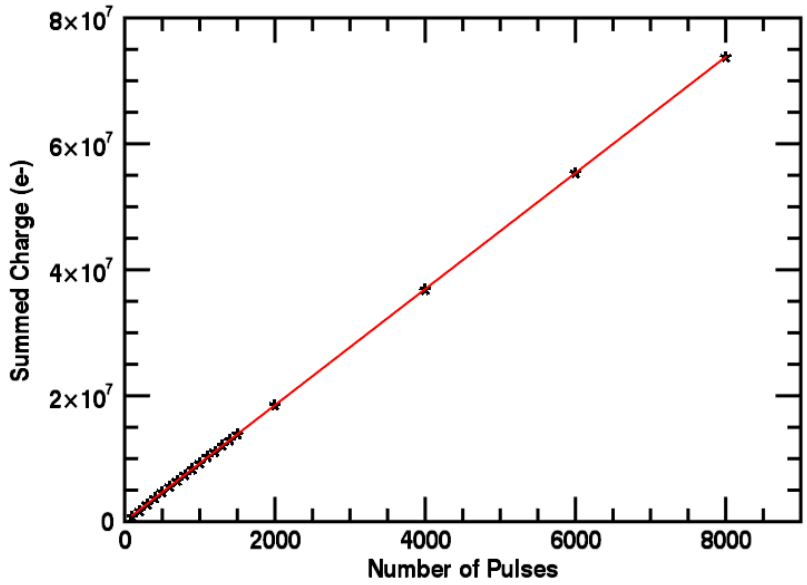

Figure 16. The summed charge in a 299x299 pixel box as the intensity is increased over 60x full well capacity.

ACKNOWLEDGEMENTS

This work was made possible by the funding from NASA contract number NNG14FC03C.

REFERENCES

[1] Downing, M., Baade, D., Sinclaire, P., et al., "CCD riddle: a) signal vs time: linear; b) singal vs variance: non-linear," Proc. SPIE 6276, 627609 (2006).
[2] Grant, C.E., Bautz, M.W., Ford, P.G., Plucinsky,P.P., "Fifteen years of the advanced CCD imaging spectrometer, " Proc. SPIE 9144, 91443Q (2014).
[3] Green, K.S., Szebenyi, D.M.E., Boggs, K., et al., "A prototype direct-detection CCD for protein crystallography," IUCr 46, 1038-1048 (2013).
[4] Guyonnet, A., Astier, P., Antilogus, P., et al., "Evidence for self-interaction of charge distribution in charge-couples devices," A&A 575, A41 (2015).
[5] Janesick, J. R., [Photon Transfer], SPIE Publications, 49-71 (2007).
[6] Janesick, J. R., [Scientific Charge-Coupled Devices], SPIE Publications, 167-382 (2001).
[7] Ricker, G. R., Winn, J. N., Vanderspek, R., et al., "The Transiting Exoplanet Survey Satellite," J. Ast. Inst. Sys. 1, 014003 (2015).

[8] Suntharalingam, V., Prigozhin, I., Young, D. J., et al., "Deep depletion CCD detectors for the transiting exoplanet survey satellite," Proc SPIE 9915, 9915-28 (2016).
[9] Westhoff, R.C., Burke, B.E., Clark, H.R., et al., "Low dark current, back-Illuminated charge-coupled devices," Proc. SPIE 7249, 7249J (2009).
[10] Woods, D. F., Vanderspek, R., MacDonald, R. et al., "The TESS Camera: Modeling and Measurements with Deep Depletion Devices," Proc SPIE 9904, 9904-77 (2015).